

Sensitivity to longitudinal vector boson scattering and doubly-charged Higgs production in $W^\pm W^\pm jj$ at future hadron colliders

Aram Apyan and Samuel Kelson

Department of Physics, Brandeis University, Waltham MA 02453, USA

Chilufya Mwewa and Marc-André Pleier

*Physics Department, Brookhaven National Laboratory,
Upton, New York 11973-5000, USA*

Luka Nedic

Department of Physics, Oxford University, Oxford OX1 3PJ, UK

Karolos Potamianos

Department of Physics, University of Warwick, Coventry; United Kingdom

(Dated: January 30, 2025)

Abstract

We study the sensitivity to longitudinal vector boson scattering at a 27, 50 and 100 TeV pp collider using events containing two leptonically-decaying same-electric-charge W bosons produced in association with two jets. Additionally, expected limits are set on doubly charged Higgs bosons produced via vector boson fusion processes and decaying to same-sign W boson pairs.

To be submitted to Physical Review D

I. INTRODUCTION

Vector boson scattering (VBS) processes are important probes of the non-Abelian gauge structure of the electroweak (EW) interactions and the EW symmetry breaking mechanism. The unitarity of the tree-level amplitude of the scattering of longitudinally polarized gauge bosons at high energies [1–3] *could* be restored by the Higgs-like boson observed at the CERN Large Hadron Collider (LHC) with a mass of about 125 GeV [4, 5]. However, modifications of the cross sections of processes involving scattering of longitudinally polarized gauge bosons with respect to the Standard Model (SM) expectations are predicted in physics beyond the SM models via the presence of additional new resonances or via modifications of the Higgs boson couplings to gauge bosons [6–8].

The VBS processes at proton-proton (pp) colliders are characterized by the presence of two gauge bosons in association with a forward/backward pair of jets. The goal of this paper is to study the prospects for measuring the polarized scattering of same-electric-charge (same-sign) $W^\pm W^\pm jj$ production at a future high energy pp machine [9, 10]. In particular, our studies focus on future hadron colliders operating at a center-of-mass energy (\sqrt{s}) of 27, 50 and 100 TeV (corresponding respectively to the High-Energy LHC (HE-LHC) using advanced high-field dipole magnets, an FCC-like ring using LHC magnet technology, and to the envisioned FCC-hh collider [9]) with an integrated luminosity of 30 ab^{-1} . The leptonic decay mode of EW production of same-sign $W^\pm W^\pm jj$, where both W bosons decay into electrons or muons (including those coming from tau leptons) and their respective (anti-) neutrinos, is a promising final state as the ratio between the strong (QCD-induced) and electroweak production of $W^\pm W^\pm jj$ is small. The ATLAS and CMS Collaborations have measured EW $W^\pm W^\pm jj$ production at $\sqrt{s} = 8$ and 13 TeV [11–15].

The W boson can be polarized either longitudinally (W_L) or transversely (W_T). This leads to three contributions, $W_L^\pm W_L^\pm jj$, $W_L^\pm W_T^\pm jj$ (which includes $W_T^\pm W_L^\pm jj$), and $W_T^\pm W_T^\pm jj$ to the overall $W^\pm W^\pm jj$ production. In this study, the candidate $W^\pm W^\pm jj$ events contain exactly two leptons with the same electric charge, missing transverse momentum, and two jets with a large rapidity separation and a high dijet invariant mass. The helicity eigenstates are defined in the WW center-of-mass reference frame which has a higher contribution from longitudinally polarized W bosons compared to the center-of-mass frame of the colliding partons. Studies of changes in polarization fractions and in kinematic distributions

arising from defining the helicity eigenstates in different reference frames at the LHC are reported in Ref. [16]. A maximum-likelihood fit is performed using the distribution of events as a function of a Boosted Decision Tree (BDT) variable optimized to distinguish between signal and background processes that can mimic the signal signature, to extract the cross sections of the $W_L^\pm W_L^\pm jj$, $W_L^\pm W_T^\pm jj$, and $W_T^\pm W_T^\pm jj$ contributions.

A first measurement attempt of the production cross sections of polarized scattering in the same-sign $W^\pm W^\pm jj$ process was performed at the LHC by the CMS Collaboration using a data sample corresponding to an integrated luminosity of 137 fb^{-1} at $\sqrt{s} = 13 \text{ TeV}$ [17], with an observed significance of about one standard deviation for the $W_L^\pm W_L^\pm jj$ component. There have been a number of studies focusing on techniques to maximize the sensitivity to the purely longitudinal contributions at the High-Luminosity LHC (HL-LHC) [18–21]. The CMS Collaboration recently projected the result in Ref. [17] to an integrated luminosity of 3000 fb^{-1} , expected at the end of the HL-LHC, to obtain an expected significance of about four standard deviations for $W_L^\pm W_L^\pm jj$ production [22]. Beyond the LHC, studies focusing on the prospects of measuring longitudinally polarized ZZ scattering at a future high-energy muon collider were performed in Ref. [23].

Some models beyond the SM predict charged Higgs bosons that couple to W and Z bosons at tree level. One such model is the Georgi-Machacek (GM) model [24]. This study sets expected limits on the production of doubly charged Higgs bosons produced via vector boson fusion processes and decaying to same-sign W boson pairs in the context of the GM model as a benchmark for Beyond the SM (BSM) sensitivity. Both the CMS and ATLAS collaborations have recently published limits on this process using data samples corresponding to 137 fb^{-1} [25] and 139 fb^{-1} [26], respectively, at $\sqrt{s} = 13 \text{ TeV}$. The ATLAS collaboration reported an excess of events corresponding to two and a half standard deviations for a doubly charged Higgs boson with a mass of 450 GeV .

II. EVENT SIMULATION

Signal events are modeled at leading order (LO) in QCD using the Monte Carlo event generator MADGRAPH5_aMC@NLO version 3.4.1 [27, 28] with the next-to-next-to-LO (NNLO) hessian NNPDF3.1 PDF set [29] interfaced with PYTHIA version 8.306 [30] for parton showering. Events where either both W bosons are longitudinally polarized ($W_L^\pm W_L^\pm jj$ events),

both W bosons are transversely polarized ($W_T^\pm W_T^\pm jj$ events), or those where one of the W bosons is longitudinally polarized and the other is transversely polarized ($W_L^\pm W_T^\pm jj$ events) are generated separately. Recent calculations of the fixed-order NLO EW and QCD corrections for the production of polarized EW $W^\pm W^\pm jj$ process at $\sqrt{s} = 13$ TeV show a significant reduction of the LO cross sections [31]. The impact is larger in high-energy tails of distributions. These calculations are not available at center-of-mass energies considered here and the investigation of the impact of the higher order corrections for these processes is beyond the scope of this work.

Background processes considered in this analysis include the production of $W^\pm W^\pm jj$ via the strong interaction, the production of $WZjj$ via the electroweak and strong interactions, and the production of $t\ell^+\ell^-j$, referred to as tZq. These processes are simulated with MADGRAPH5_aMC@NLO as well.

The Delphes [32] program, using a generic Future Circular Collider (FCC) detector card [33], is then used to simulate detector effects for all samples. Jets are clustered from the reconstructed objects using FASTJET [34] with the anti-kt clustering algorithm [35], and a distance parameter of 0.4. For the validation of the signal samples, an inclusive $W^\pm W^\pm jj$ electroweak sample was generated using the same generator and settings as well as Delphes for detector effects, and good agreement was observed with respect to the sum of the polarized signal samples. Detector-specific backgrounds such as those in which lepton charge is misidentified or those in which jets mimic leptons were not considered in this analysis as they are highly detector-specific.

III. EVENT SELECTION

Signal ($W^\pm W^\pm jj$) events are characterized by the presence of two high transverse momentum (p_T) same-charge leptons (electrons or muons, denoted by ℓ), large missing transverse momentum (E_T^{miss}) and two forward/backward jets with large di-jet invariant mass (M_{jj}). In this analysis, events with τ leptons are only considered when the τ decays leptonically (to e or μ). For simplicity, the event selection was optimised for $\sqrt{s} = 100$ TeV to maximize the background rejection and enhance the signal and then applied to all \sqrt{s} values under study. The di-lepton invariant mass ($M_{\ell\ell}$) was required to be at least 60 GeV in order to minimize the background contribution from low mass Drell-Yan processes. To eliminate leptons from

Z bosons, the invariant mass of a pair of electrons or muons was required to be away from the Z mass by at least 10 GeV. A large di-jet invariant mass of at least 2 TeV was required in order to satisfy the VBS topology. Table I gives a summary of all object and event selection cuts applied in this analysis. The distributions of events as a function of the separation in azimuthal angle ϕ between the two leading jets in p_T ($\Delta\phi_{jj}$) are shown in Figure 1 for all the three center-of-mass energies.

Selection type	Requirement
Number of leptons	Exactly 2 same-charge leptons
Lepton p_T	$p_T \geq 15$ GeV
Number of jets	≥ 2
Jet p_T	$p_T \geq 50$ GeV
Di-lepton invariant mass	$M_{ll} \geq 60$ GeV
Z-veto	$ M_{ll} - M_Z > 10$ GeV
Di-jet invariant mass	$M_{jj} \geq 2$ TeV
Missing transverse momentum	$E_T^{miss} \geq 50$ GeV

TABLE I. Selection criteria used for $W^\pm W^\pm jj$ events.

IV. THEORY UNCERTAINTIES

There are three primary sources of theoretical uncertainties associated with perturbative QCD matrix-element calculations. The first and largest is due to the missing higher-order terms in perturbative expansions. To estimate this uncertainty, samples are generated with variations of the renormalization (μ_R) and factorization (μ_F) scales. Pairwise variations of up to a factor of 2 are performed in the up and down direction $\{\mu_R, \mu_F\} \times \{0.5, 0.5\}, \{1, 0.5\}, \{0.5, 1\}, \{1, 1\}, \{2, 1\}, \{1, 2\}, \{2, 2\}$, with the final uncertainty evaluated by taking the envelope of all 7-point scale variations. In addition to the scale variations, PDF and α_S uncertainties also contribute to the theoretical uncertainty. The theoretical uncertainty associated with the PDF is evaluated by varying the internal parameters following the prescription from [36]. Finally, the third source of theoretical uncertainty is associated with the determination of the strong coupling constant, α_S . The coupling constant

is determined experimentally using fixed-order calculations in perturbation theory. The α_S uncertainties are evaluated at two different α_S values and the uncertainty is calculated following the recommendations of [36].

\sqrt{s} (TeV)	$W_L W_L$	$W_L W_T$	$W_T W_T$	WW QCD	tZq	WZ EW	WZ QCD
27	14.7	15.4	15.8	23.7	10.4	16.3	52.0
50	10.8	9.99	10.1	18.4	10.3	11.1	37.6
100	4.92	5.32	5.40	13.0	10.4	5.48	30.8

TABLE II. Relative percentage effect on the event yields of the theory systematics for each sample.

Table II summarizes the effect of theory uncertainties on their respective sample as a relative percentage of the total event yield. The systematics have the largest impact on the 27 TeV samples, with the effects decreasing with center-of-mass energy. The largest source of uncertainty for all center-of-mass energies arises from the scale uncertainties on the QCD-induced WZ background.

V. SENSITIVITY TO $W^\pm W^\pm jj$ POLARIZATIONS

To separate the three $W^\pm W^\pm jj$ polarizations from background processes, two Boosted Decision Trees (BDTs) were trained using XGBoost [37]. The first BDT separates the $W^\pm W^\pm jj$ signal from the background processes (referred to as SB BDT) and the second BDT separates the three $W^\pm W^\pm jj$ polarization states (referred to as Pol BDT). Several kinematic variables were used as input to the BDTs, as can be seen in Table III. This subset of variables for training was chosen from a larger set based on performance. Additionally, a correlation coefficient matrix was generated. The top 15 of the initial 25 variables were kept while avoiding keeping multiple variables with high correlations with respect to each other. Hyperparameters, including the learning rate, maximum depth, subsample ratio, and number of estimators, were tuned via a random grid search algorithm [38]. Simulated MC events were split into training and testing samples used for validation.

The Pol BDT is a multi-class classifier consisting of three outputs. Each output corresponds to a classification probability associated with one of the polarization states. The SB BDT is a binary classifier, with a single output giving the classification probability of

Variable	Description	SB	Pol
$ \Delta\eta_{\ell\ell} $	Difference in rapidity of the leading and sub-leading leptons		✓
$ \Delta\phi_{\ell_0 E_{\text{miss}}^T} $	Difference in azimuthal angles of the leading lepton and missing transverse energy		✓
$ \Delta\phi_{\ell_1 E_{\text{miss}}^T} $	Difference in azimuthal angles of the sub-leading lepton and missing transverse energy	✓	✓
$ \Delta\phi_{\ell_0\ell_1} $	Difference in azimuthal angles of the leading and sub-leading leptons		✓
$ \Delta\phi_{\ell\ell E_{\text{miss}}^T} $	Difference in azimuthal angles of the dilepton system and missing transverse energy	✓	
$ \Delta R_{j_1\ell_1} $	Distance between the leading jet and leading lepton		✓
$ \Delta R_{j_2\ell_2} $	Distance between the sub-leading jet and sub-leading lepton	✓	
$ \Delta R_{jj} $	Distance between the leading jet and sub-leading jet	✓	✓
E_{miss}^T	Missing transverse energy	✓	✓
m_{jj}	Mass of the dijet system	✓	
$m_{\ell\ell}$	Mass of the dilepton system	✓	✓
p_{Tj_1}	Transverse momentum of the leading jet	✓	
p_{Tj_2}	Transverse momentum of the sub-leading jet	✓	
p_{Tj_3}	Transverse momentum of the 3rd leading jet	✓	✓
p_{Tjj}	Transverse momentum of the dijet system		✓
$p_{T\ell_1}$	Transverse momentum of the leading lepton	✓	✓
$p_{T\ell_2}$	Transverse momentum of the sub-leading lepton		✓
$p_{T\text{rel}}$	Transverse momentum ratios for leptons and jets	✓	✓
$\sum\eta_{\ell}$	Sum of rapidity of all leptons	✓	
$\text{Zeppenfeld}_{\ell_1}$	Zeppenfeld variable for the leading lepton	✓	✓
$\text{Zeppenfeld}_{\ell_2}$	Zeppenfeld variable for the sub-leading lepton	✓	

TABLE III. Variables, their descriptions, and which BDT they were used in.

an inclusive $W^{\pm}W^{\pm}jj$ event. The two BDTs are combined within the analysis framework to generate a three-dimensional histogram. The x and y dimensions present the predicted

probability of observing a longitudinal-longitudinal and transverse-transverse event coming from the output of the polarization BDT, and the z dimension presents the probability of an inclusive $W^\pm W^\pm jj$ signal event coming from the SB BDT. As the sum of the predicted probability of the Pol BDT is equal to one, only two outputs are necessary for complete sensitivity to polarization. The three-dimensional BDT is “unrolled” to form a one-dimensional histogram. The unrolling translates each individual bin in the three-dimensional histogram to an individual bin in a one-dimensional histogram.

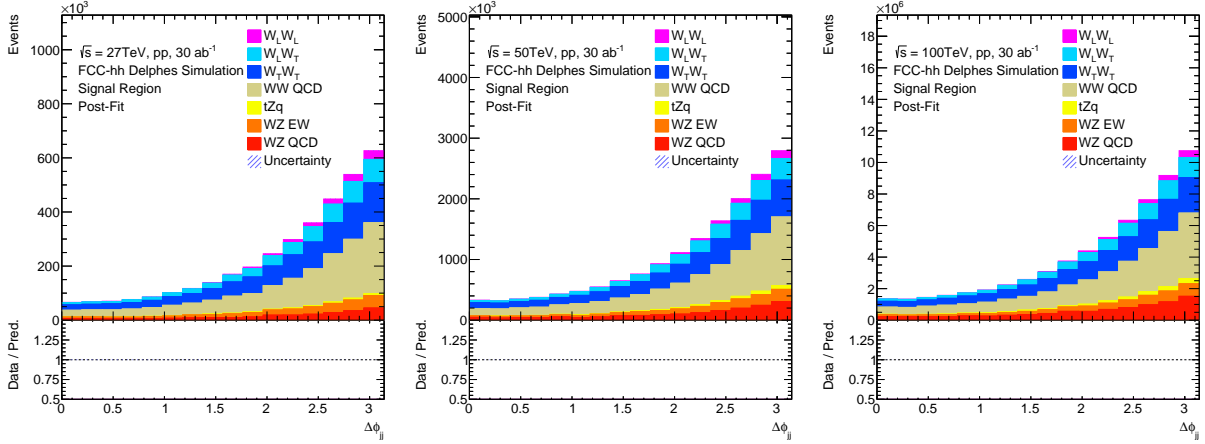


FIG. 1. The post-fit distribution of events as a function of $\Delta\phi_{jj}$.

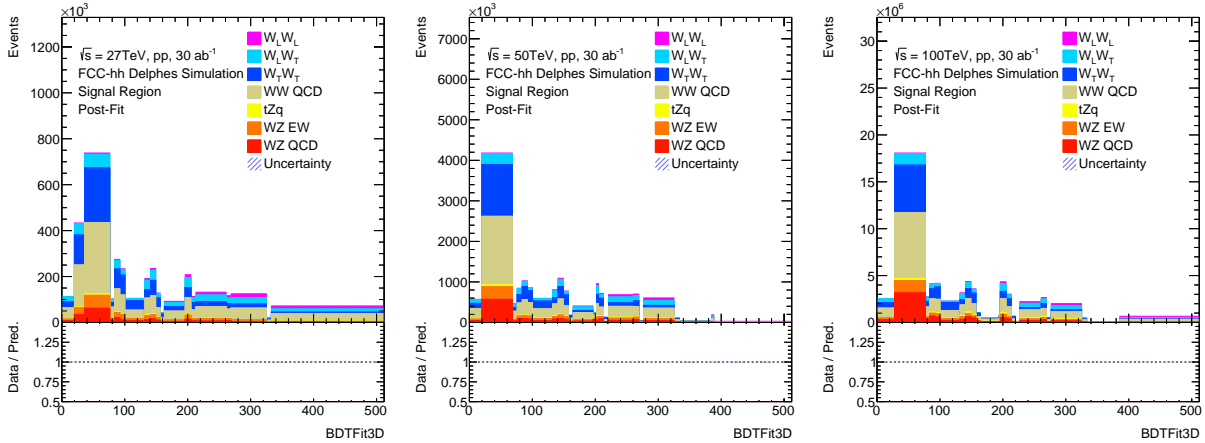


FIG. 2. The post-fit distribution of events as a function of the unrolled BDT (BDTFit3D).

The expected sensitivity to the $W^\pm W^\pm jj$ polarization contributions is estimated using a profile likelihood fit as implemented in the RooFit [39] and RooStats [40] packages. We consider three signal strength parameters, μ_{LL} , μ_{LT} and μ_{TT} corresponding to each of the

$W^\pm W^\pm jj$ polarization states. In addition to the theoretical uncertainties, we assume a normalization uncertainty of 2% for all the processes due to uncertainties in the integrated luminosity. The uncertainties associated with the limited number of simulated events are also included in the profile likelihood fit. We do not consider other sources of experimental systematic uncertainties in this study.

The sensitivity is measured for two distributions: $\Delta\phi_{jj}$ and the three-dimensional BDT. The $\Delta\phi_{jj}$ distribution is used as a baseline benchmark for the sensitivity to polarization and as a comparison to illustrate the improvements when applying multivariate analysis techniques such as BDTs. Before fitting, the BDT distributions are also subject to a binning optimization procedure. The procedure requires a fixed minimum of background and signal events per bin, as well as a minimum of 200 events per background. The procedure then iteratively tests merged bin configurations and compares each configuration by calculating the significance before and after merging. The binning configuration with the smallest number of bins, with the best significance, is taken as final. The significance is estimated as described in [41]. The post-fit distributions for $\Delta\phi_{jj}$ and the BDT following the binning optimization procedure are shown in Figures 1 and 2.

Polarization	Signal Strength: BDT		
	$\sqrt{s} = 27$ TeV	$\sqrt{s} = 50$ TeV	$\sqrt{s} = 100$ TeV
μ_{LL}	1 ± 0.22	1 ± 0.21	1 ± 0.15
μ_{LT}	1 ± 0.13	1 ± 0.095	1 ± 0.096
μ_{TT}	1 ± 0.13	1 ± 0.085	1 ± 0.045
	Signal Strength: $\Delta\phi_{jj}$		
μ_{LL}	1 ± 1.02	1 ± 0.62	1 ± 0.40
μ_{LT}	1 ± 0.45	1 ± 0.42	1 ± 0.14
μ_{TT}	1 ± 0.33	1 ± 0.26	1 ± 0.12

TABLE IV. Signal strengths μ after the $\Delta\phi_{jj}$ and BDT fit for each $W^\pm W^\pm jj$ polarization state and all \sqrt{s} values under study.

Table IV shows the signal strengths μ , defined as the ratio of the fitted to the expected SM cross-section, and the corresponding uncertainties for each $W^\pm W^\pm jj$ polarization state for all the considered \sqrt{s} values. The values are expected to be unity because the Asimov

dataset [42] is used in the fit. The breakdown of the uncertainties on the purely longitudinal scattering signal strength parameter is shown in Equation 1 where “stat” refers to the contribution of the statistical uncertainty to the overall uncertainty and “syst” refers to the contribution of the systematic uncertainties, which include theoretical and luminosity uncertainties, as well as statistical uncertainties arising from limited number of MC events.

$$\begin{aligned}
\mu_{LL}^{27 \text{ TeV}} &= 1.00 \pm 0.22 = 1 \pm 0.17 \text{ (stat.)} \pm 0.14 \text{ (syst.)} \\
\mu_{LL}^{50 \text{ TeV}} &= 1.00 \pm 0.21 = 1 \pm 0.18 \text{ (stat.)} \pm 0.11 \text{ (syst.)} \\
\mu_{LL}^{100 \text{ TeV}} &= 1.00 \pm 0.15 = 1 \pm 0.12 \text{ (stat.)} \pm 0.09 \text{ (syst.)}
\end{aligned}
\tag{1}$$

VI. LIMITS ON DOUBLY-CHARGED HIGGS BOSON PRODUCTION

Charged Higgs bosons with couplings to W and Z bosons are included at tree level in extended Higgs sectors with additional isotriplet scalar fields [43]. In this study, we use the same-sign WW signal region described in Section III to set limits on doubly charged Higgs bosons produced via Vector Boson Fusion (VBF). This is done in the context of the Georgi-Machacek model [24] in which two isospin triplet scalar fields are added to the SM Higgs doublet. One of the constituents of the scalar potential is a quintuplet of Higgs bosons; $H_5^{\pm\pm}$, H_5^\pm , and H_5^0 of common mass, $m_{H_5^{\pm\pm}}$, that couple to W and Z bosons. Our interpretation uses the H5 plane benchmark hypothesis of the GM model which was developed by the Higgs cross section working group at the Large Hadron Collider (LHC) [43]. In this benchmark, doubly charged Higgs bosons ($H_5^{\pm\pm}$) decay to pairs of same-sign W bosons with a branching fraction of 100%. The production and decay of the $H_5^{\pm\pm}$ states depend on two parameters; the mass, $m_{H_5^{\pm\pm}}$, and the $\sin\theta_H$ (or s_H) parameter characterising the contribution of isospin triplet scalar fields to the W and Z boson masses. The decay widths are proportional to s_H^2 .

Signal samples were simulated using MADGRAPH5_aMC@NLO version 3.4.1 [27, 28] at LO with the NNLO hessian NNPDF3.1 PDF set [29] interfaced with PYTHIA version 8.306 [30] for parton showering. The Delphes [32] program, using a generic FCC detector card [33], was then used to simulate detector effects. Five $H_5^{\pm\pm}$ mass points were simulated: 800 GeV, 900 GeV, 1000 GeV, 2000 GeV, and 3000 GeV. The high-mass region was selected due to the stringent limits already established by LHC experiments in the low mass region. Since

$H_5^{\pm\pm}$ decay widths are proportional to $m_{H_5^{\pm\pm}}$ and s_H^2 , s_H values were set to 0.5 for the 800 GeV mass point, and to 0.25 for the higher masses.

To extract the limits, we performed a binned maximum-likelihood fit to the transverse mass (m_T) distribution of the di-lepton and E_{miss}^T system which effectively distinguishes between the resonant signal and background processes. In addition to statistical uncertainties, systematic uncertainties, which include a 2% uncertainty on the luminosity, MC statistical uncertainties arising from a limited number of MC events, as well as theory uncertainties described in Section IV, were considered in this fit. Limits were extracted at 95% CL using the CL_s technique [44].

Figure 3 shows m_T post-fit distributions for the 2000 GeV $H_5^{\pm\pm}$ mass point in the signal region. Expected upper limits on the s_H parameter as a function of $m_{H_5^{\pm\pm}}$ are shown in Figure 4. Upper limits with and without systematic uncertainties are shown. In general, for the 100 TeV center-of-mass energy, these upper limits range between 0.14-0.25 (with systematic uncertainties) and 0.02-0.04 (without systematic uncertainties). The strong expected upper limits in the latter case is mainly due to the statistical uncertainties arising from the limited number of MC events. In addition, expected upper limits on $\sigma(H_5^{\pm\pm}) \times \mathcal{B}(H_5^{\pm\pm} \rightarrow W^\pm W^\pm)$ are also shown.

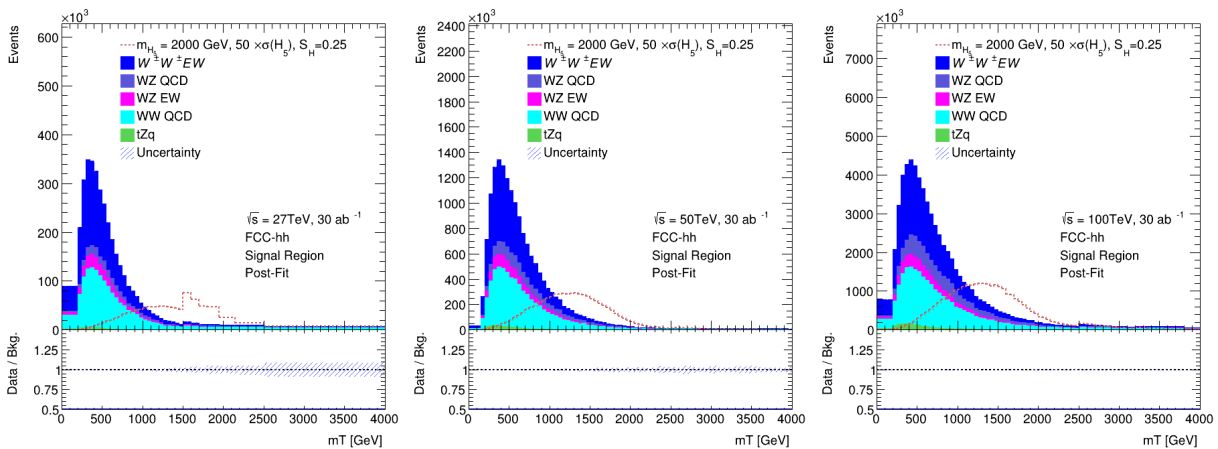


FIG. 3. Post-fit m_T distributions for the 2000 GeV $H_5^{\pm\pm}$ signal at the three FCC-hh center-of-mass energy scenarios; 27 TeV (left), 50 TeV (center) and 100 TeV (right). The bins are optimized to ensure a minimum of 100 background events per bin, resulting in variable bin sizes.

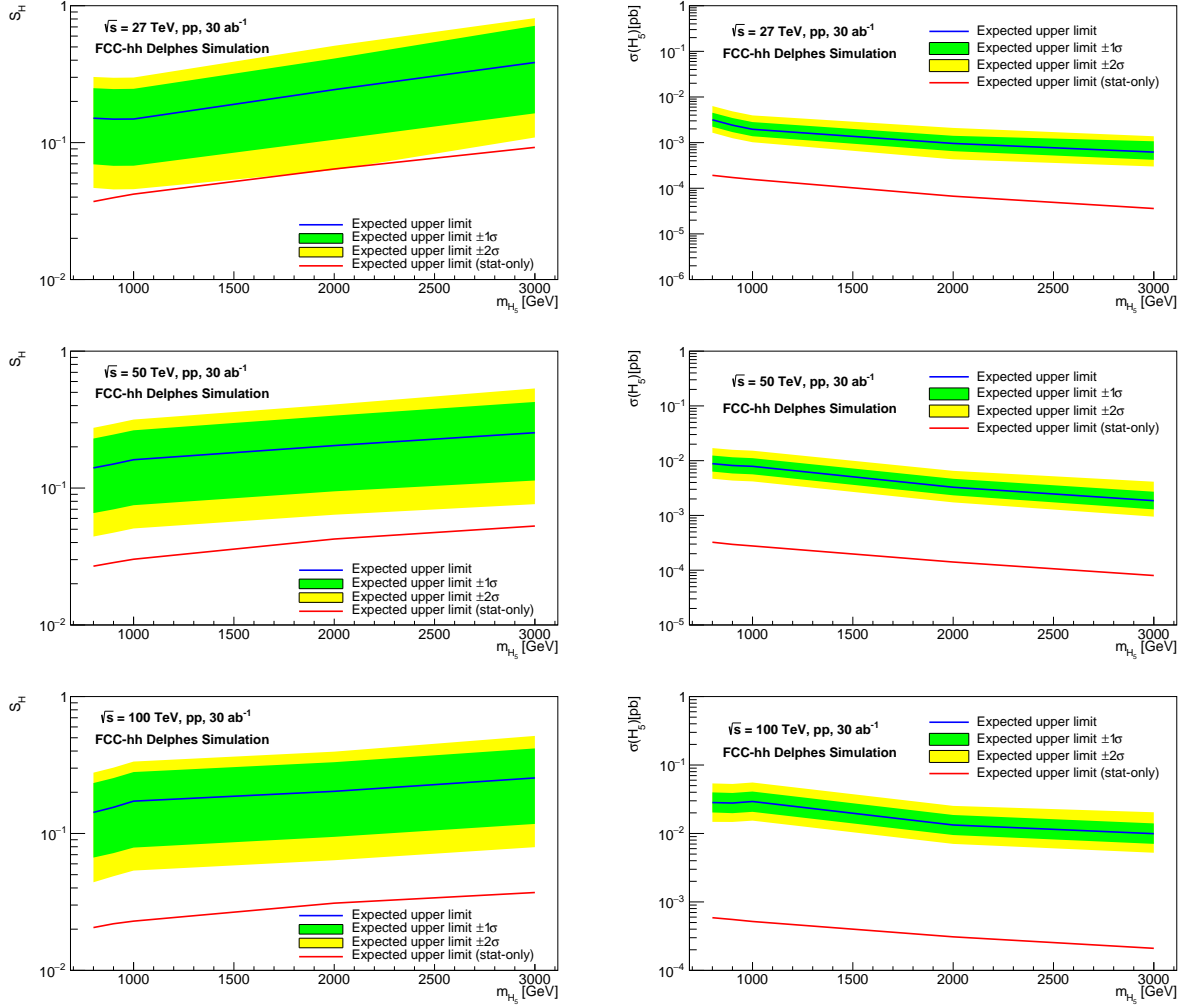


FIG. 4. Expected exclusion limits at 95% CL on s_H (left) and $\sigma(H_5^{\pm\pm}) \times \mathcal{B}(H_5^{\pm\pm} \rightarrow W^\pm W^\pm)$ (right) as a function of $m_{H_5^{\pm\pm}}$ at the three center of mass energy scenarios: 27 TeV (top), 50 TeV (center) and 100 TeV (bottom). The blue solid line indicates exclusion limits with both statistical and systematic uncertainties included whereas the red solid line indicates exclusion limits without systematic uncertainties. The green and yellow bands indicate the 68% and 95% confidence intervals around the median limits, respectively.

VII. CONCLUSIONS

Cross section measurements of the polarized scattering of same-sign $W^\pm W^\pm jj$ production using the leptonic decay mode at a future high energy pp collider with an integrated luminosity of 30 ab^{-1} should be possible with a relative precision of around 22% at $\sqrt{s} = 27 \text{ TeV}$, 21% at $\sqrt{s} = 50 \text{ TeV}$ and 15% at $\sqrt{s} = 100 \text{ TeV}$ for the purely longitudinal contribution

and better for the other contributions. An interpretation of the results in the context of the Georgi-Machacek model yields expected exclusion limits on the s_H parameter as a function of $m_{H_5^{\pm\pm}}$. In general, for the 50 TeV and 100 TeV center of mass energies, s_H parameter values greater than 0.14-0.25 are expected to be excluded with the results limited by the number of MC events available for this study.

ACKNOWLEDGMENTS

The work of A.A. is supported by the U.S. Department of Energy, Office of Science, Office of High Energy Physics under contract no. DE-SC0013542. The work of C.M. and M.-A.P. is supported by the U.S. Department of Energy, Office of Science, Office of High Energy Physics under contract no. DE-SC0012704. The work of K.P. and L.N. is supported by the U.K. Research and Innovation Science and Technology Facilities Council, under project no. ST/T004568/1 and 2422336, respectively.

-
- [1] M. J. G. Veltman, “Second Threshold in Weak Interactions,” *Acta Phys. Pol. B*, vol. 8, p. 475, 1977.
 - [2] B. W. Lee, C. Quigg, and H. B. Thacker, “The strength of weak interactions at very high-energies and the Higgs boson mass,” *Phys. Rev. Lett.*, vol. 38, p. 883, 1977.
 - [3] B. W. Lee, C. Quigg, and H. B. Thacker, “Weak interactions at very high-energies: the role of the Higgs boson mass,” *Phys. Rev. D*, vol. 16, p. 1519, 1977.
 - [4] ATLAS Collaboration, “Observation of a new particle in the search for the Standard Model Higgs boson with the ATLAS detector at the LHC,” *Phys. Lett. B*, vol. 716, p. 1, 2012.
 - [5] CMS Collaboration, “Observation of a new boson at a mass of 125 GeV with the CMS experiment at the LHC,” *Phys. Lett. B*, vol. 716, p. 30, 2012.
 - [6] D. Espriu and B. Yencho, “Longitudinal WW scattering in light of the Higgs boson discovery,” *Phys. Rev. D*, vol. 87, p. 055017, 2013.
 - [7] J. Chang, K. Cheung, C.-T. Lu, and T.-C. Yuan, “WW scattering in the era of post-Higgs-boson discovery,” *Phys. Rev. D*, vol. 87, p. 093005, 2013.

- [8] S. J. Lee, M. Park, and Z. Qian, “Probing unitarity violation in the tail of the off-shell Higgs boson in $V_L V_L$ mode,” *Phys. Rev. D*, vol. 100, p. 011702, 2019.
- [9] A. Abada *et al.*, “FCC-hh: The Hadron Collider: Future Circular Collider Conceptual Design Report Volume 3,” *Eur. Phys. J. ST*, vol. 228, p. 755, 2019.
- [10] “CEPC Conceptual Design Report: Volume 1 - Accelerator,” 9 2018.
- [11] ATLAS Collaboration, “Evidence for Electroweak Production of $W^\pm W^\pm jj$ in pp Collisions at $\sqrt{s} = 8$ TeV with the ATLAS Detector,” *Phys. Rev. Lett.*, vol. 113, p. 141803, 2014.
- [12] CMS Collaboration, “Study of vector boson scattering and search for new physics in events with two same-sign leptons and two jets,” *Phys. Rev. Lett.*, vol. 114, p. 051801, 2015.
- [13] CMS Collaboration, “Observation of Electroweak Production of Same-Sign W Boson Pairs in the Two Jet and Two Same-Sign Lepton Final State in Proton–Proton Collisions at $\sqrt{s} = 13$ TeV,” *Phys. Rev. Lett.*, vol. 120, p. 081801, 2018.
- [14] ATLAS Collaboration, “Observation of Electroweak Production of a Same-Sign W Boson Pair in Association with Two Jets in pp Collisions at $\sqrt{s} = 13$ TeV with the ATLAS Detector,” *Phys. Rev. Lett.*, vol. 123, p. 161801, 2019.
- [15] CMS Collaboration, “Measurements of production cross sections of WZ and same-sign WW boson pairs in association with two jets in proton–proton collisions at $\sqrt{s} = 13$ TeV,” *Phys. Lett. B*, vol. 809, p. 135710, 2020.
- [16] A. Ballestrero, E. Maina, and G. Pelliccioli, “Different polarization definitions in same-sign WW scattering at the LHC,” *Phys. Lett. B*, vol. 811, p. 135856, 2020.
- [17] CMS Collaboration, “Measurements of production cross sections of polarized same-sign W boson pairs in association with two jets in proton–proton collisions at $\sqrt{s} = 13$ TeV,” *Phys. Lett. B*, vol. 812, p. 136018, 2021.
- [18] J. Searcy, L. Huang, M.-A. Pleier, and J. Zhu, “Determination of the WW polarization fractions in $pp \rightarrow W^\pm W^\pm jj$ using a deep machine learning technique,” *Phys. Rev. D*, vol. 93, p. 094033, 2016.
- [19] J. Lee, N. Chanon, A. Levin, J. Li, M. Lu, Q. Li, and Y. Mao, “Polarization fraction measurement in same-sign WW scattering using deep learning,” *Phys. Rev. D*, vol. 99, no. 3, p. 033004, 2019.
- [20] P. Azzi *et al.*, “Standard Model Physics at the HL-LHC and HE-LHC,” *arXiv:1902.04070*, 2018.

- [21] J. Roloff, V. Cavaliere, M.-A. Pleier, and L. Xu, “Sensitivity to longitudinal vector boson scattering in semileptonic final states at the HL-LHC,” *Phys. Rev. D*, vol. 104, p. 093002, 2021.
- [22] CMS Collaboration, “Prospects for the measurement of vector boson scattering production in leptonic $W^\pm W^\pm$ and WZ diboson events at $\sqrt{s} = 14$ TeV at the High-Luminosity LHC,” tech. rep., CERN, Geneva, 2021.
- [23] T. Yang, S. Qian, Z. Guan, C. Li, F. Meng, J. Xiao, M. Lu, and Q. Li, “Longitudinally polarized ZZ scattering at a muon collider,” *Phys. Rev. D*, vol. 104, p. 093003, 2021.
- [24] H. Georgi and M. Machacek, “Doubly charged Higgs bosons,” *Nuclear Physics B*, vol. 262, no. 03, pp. 463–477, 1985.
- [25] CMS Collaboration, “Search for charged Higgs bosons produced in vector boson fusion processes and decaying into vector boson pairs in proton–proton collisions at $\sqrt{s} = 13$ TeV,” *Eur. Phys. J. C*, vol. 81, p. 723, 2021.
- [26] ATLAS Collaboration, “Measurement and interpretation of same-sign W boson pair production in association with two jets in pp collisions at $\sqrt{s} = 13$ TeV with the ATLAS detector,” *JHEP*, vol. 04, p. 026, 2024.
- [27] J. Alwall *et al.*, “The automated computation of tree-level and next-to-leading order differential cross sections, and their matching to parton shower simulations,” *JHEP*, vol. 07, no. 79, 2014.
- [28] D. Buarque Franzosi, O. Mattelaer, R. Ruiz, and S. Shil, “Automated predictions from polarized matrix elements,” *JHEP*, vol. 04, p. 082, 2020.
- [29] R. D. Ball, V. Bertone, S. Carrazza, L. D. Debbio, S. Forte, P. Groth-Merrild, A. Guffanti, N. P. Hartland, Z. Kassabov, J. I. Latorre, E. R. Nocera, J. Rojo, L. Rottoli, E. Slade, and M. Ubiali, “Parton distributions from high-precision collider data: NNPDF Collaboration,” *The European Physical Journal C*, vol. 77, Oct. 2017.
- [30] C. Bierlich, S. Chakraborty, N. Desai, L. Gellersen, I. Helenius, P. Ilten, L. Lönnblad, S. Mrenna, S. Prestel, C. T. Preuss, T. Sjöstrand, P. Skands, M. Utheim, and R. Verheyen, “A comprehensive guide to the physics and usage of PYTHIA 8.3,” 2022.
- [31] A. Denner, C. Haitz, and G. Pelliccioli, “NLO EW and QCD corrections to polarised same-sign WW scattering at the LHC,” *JHEP*, vol. 11, p. 115, 2024.

- [32] J. de Favereau, C. Delaere, P. Demin, A. Giammanco, V. Lemaître, A. Mertens, and M. Selvaggi, “DELPHES 3, A modular framework for fast simulation of a generic collider experiment,” *JHEP*, vol. 02, p. 057, 2014.
- [33] M. Selvaggi, “Delphes fcc-hh card.” <https://github.com/delphes/delphes/blob/master/cards/FCC/FCCh.tcl>. Accessed: 2025.
- [34] M. Cacciari, G. P. Salam, and G. Soyez, “FastJet user manual,” *Eur. Phys. J. C*, vol. 72, p. 1896, 2012.
- [35] M. Cacciari, G. P. Salam, and G. Soyez, “The anti-kt jet clustering algorithm,” *JHEP*, vol. 04, p. 063, 2008.
- [36] J. Butterworth *et al.*, “PDF4LHC recommendations for LHC Run II,” *Journal of Physics G: Nuclear and Particle Physics*, vol. 43, p. 023001, Jan. 2016.
- [37] T. Chen and C. Guestrin, “XGBoost: A Scalable Tree Boosting System,” in *Proceedings of the 22nd ACM SIGKDD International Conference on Knowledge Discovery and Data Mining*, p. 785–794, ACM, Aug. 2016.
- [38] F. Pedregosa, G. Varoquaux, A. Gramfort, V. Michel, B. Thirion, O. Grisel, M. Blondel, P. Prettenhofer, R. Weiss, V. Dubourg, J. Vanderplas, A. Passos, D. Cournapeau, M. Brucher, M. Perrot, and E. Duchesnay, “Scikit-learn: Machine learning in Python,” *Journal of Machine Learning Research*, vol. 12, pp. 2825–2830, 2011.
- [39] W. Verkerke and D. P. Kirkby, “The RooFit toolkit for data modeling,” *eConf*, vol. C0303241, p. MOLT007, 2003.
- [40] L. Moneta, K. Belasco, K. S. Cranmer, S. Kreiss, A. Lazzaro, D. Piparo, G. Schott, W. Verkerke, and M. Wolf, “The RooStats Project,” *PoS*, vol. ACAT2010, p. 057, 2010.
- [41] ATLAS Collaboration, “Formulae for Estimating Significance,” tech. rep., 2020.
- [42] G. Cowan, K. Cranmer, E. Gross, and O. Vitells, “Asymptotic formulae for likelihood-based tests of new physics,” *Eur. Phys. J. C*, vol. 71, p. 1554, 2011.
- [43] M. Zaro and H. Logan, “Recommendations for the interpretation of LHC searches for H_5^0 , H_5^\pm and $H_5^{\pm\pm}$ in vector boson fusion with decays to vector boson pairs,” tech. rep., CERN, Geneva, 2015.
- [44] A. L. Read, “Modified frequentist analysis of search results (the CL_s method),” 2000.